

Crack initiation and growth in an Zn-Cu-Al PE alloy

**Vittorio Di Cocco^{1,*}, Francesco Iacoviello¹, Luigi Tomassi¹, Stefano Natali²,
Valerio Volpe²**

¹ Department DICeM, University of Cassino and Southern Lazio, 03043, Italy

² Department DICMA, University of Rome “Sapienza”, 00184, Italy

* Corresponding author: v.dicocco@unicas.it

Abstract Cu–Zn–Al shape memory alloys exhibit shape memory behavior within a certain range of composition. They are characterized by a stable high temperature disordered bcc structure named β -phase, followed by a transition to a B2 structure after appropriate cooling and from secondary B2 to DO3 ordering under other cooling procedures. It is also known that martensite stabilization can be reduced by a step-quenched treatment. Shape memory properties are often absolutely interesting and many grades of shape memory alloys are extensively used in the technological world, e. g. in surgery and dentistry. Copper-based shape memory alloys are preferred for their good memory properties and low cost of production.

In this work, the main crack initiation and its propagation in an tensile test is analyzed in order to evaluate crack path and its behavior corresponding to low and to high deformation values. Furthermore, results are associated to X-Ray diffraction in order to correlate structural transition involved in an Cu-Zn-Al alloy characterized by a PE behavior.

Keywords Shape Memory Alloy; Pseudo-Elastic Behaviour; Fracture; CuZnAl alloy.

1. Introduction

Shape memory alloys (SMA) and pseudo-elastic alloys (PEA) are able to recover their original shape after high mechanical deformations: the first ones by heating up to characteristic temperature (Shape Memory Effect, SME), and the second ones simply by removing the mechanical load (Pseudo-elastic Effect, PE). Different shape memory alloys have been optimized in the last decades, such as the copper-zinc-aluminum (ZnCuAl), copper-aluminum-nickel (CuAlNi), nickel-manganese-gallium (NiMnGa), nickel-titanium (NiTi), and other SMAs obtained alloying zinc, copper, gold, iron, etc.. However, the near equiatomic NiTi binary system shows the most interesting properties and it is currently used in an increasing number of applications in many fields of engineering, for the realization of smart sensors and actuators, joining devices, hydraulic and pneumatic valves, release/separation systems, consumer applications and commercial gadgets [1, 2]. Due to their good biocompatibility, another important field of SMA application is medicine, where the pseudo-elasticity is mainly exploited for the realization of several components such as cardiovascular stent, embolic protection filters, orthopedic components, orthodontic wires, micro surgical and endoscopic devices [3].

From the microstructural point of view, shape memory and pseudo-elastic effects are due to a reversible solid state microstructural transition from austenite to martensite, which can be activated by mechanical and/or thermal loads [4].

Copper-based shape-memory alloys are very sensitive to thermal effects, and it is possible that in

thermal cycles its properties change (e.g., shape-recovery ratio, transformation temperatures, crystal structures, hysteresis and mechanical behavior).

Cu–Zn–Al shape memory alloys exhibit shape memory behavior within a certain range of composition. It is characterized by a stable high temperature disordered bcc structure named β -phase. After a customized cooling process, a B2 structure is obtained followed a DO₃ ordering. It is also known that martensite stabilization can be reduced by a step-quenched treatment.

Cu ZnAl alloys mechanical properties are influenced by [5]:

- martensite stabilization;
- grain size;
- processes procedure (e.g., temperature, heat treatment cycles number).

Other investigations carried out on CuZnAl alloys, showed a strain influence on the macroscopic behavior and on martensite morphology. Martensitic transformation occurs initially in deformed material and the manufacturing shape follows the transformation [6]. Larger grain dimensions allow an easier transformation process, allowing the growth of 18R martensite [7].

In this work, damaging micromechanism during a tensile test in a CuZnAl alloy has been investigated, focusing the crack initiation and its stable growth. Deformation influence on alloy microstructure has been investigated during the tensile test by means of X-Ray diffraction .

2. Material and methods

In this work a CuZnAl pseudo-elastic alloy, made in laboratory by using controlled atmosphere furnace and characterized by chemical composition shown in Table 1, has been used to investigate mechanical behavior in tensile conditions.

Table 1. Chemical composition of CuZnAl investigated alloy

Cu	Zn	Al	Other
73.00	21.80	5.04	0.16

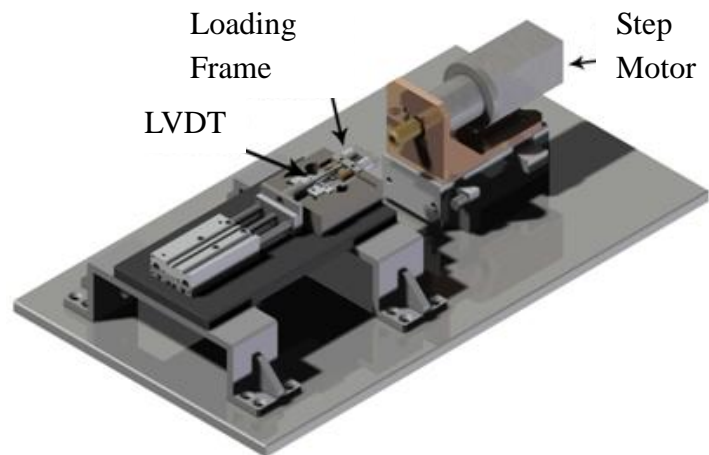
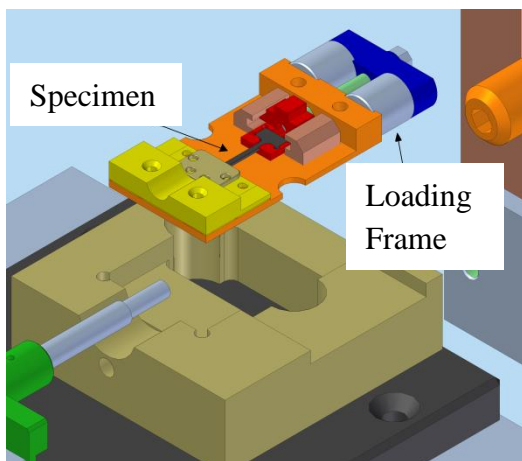
The evolution of the microstructure during uniaxial deformation was analyzed by a miniature testing machine (Fig. 1) which allows in-situ scanning electron microscopic (SEM) observations as well as X-Ray micro-diffraction analyses.

In particular, the testing machine is equipped with a simple and removable loading frame, which allows SEM and X-Ray analyses at fixed values of applied load and/or deformations. The machine is powered by a stepping motor, which applies the mechanical deformation to the specimen through a calibrated screw, with pitch of 0.8mm, and a control electronic allows simultaneous measurement and/or control of applied load and stroke of the specimen head. The stroke is measured by a Linear Variable Differential Transformer (LVDT) while the load is measured by two miniaturized load cells with maximum capacity of 10 kN. Miniature dog bone shaped specimens were machined from alloy samples obtained by cold cutting of mini sheets from as cast ingots, by wire electro discharge machining.

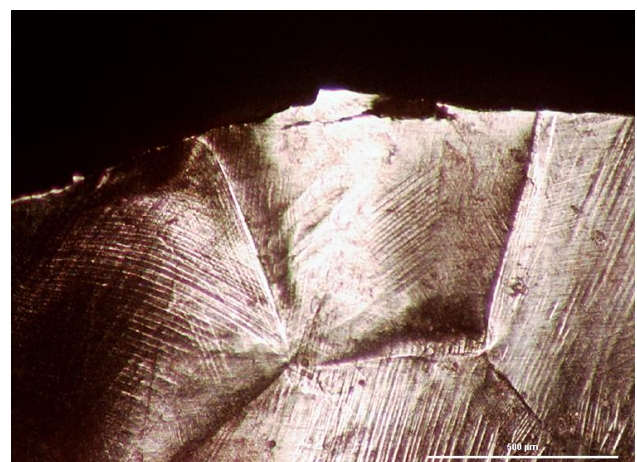
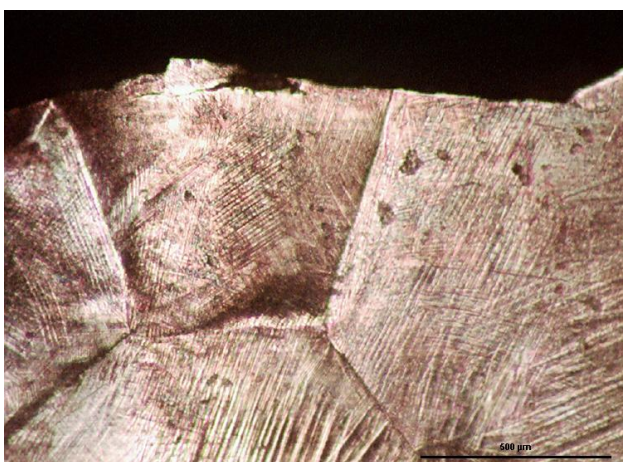
Step by step isothermal tensile tests were carried out, at room temperature, at increasing values of

the specimens elongation. For each loading step, the loading frame containing the specimen was removed from the testing machine, at fixed values of deformation. The specimens, under load condition, was analyzed by means of:

- 1) a light optical microscope, characterized by a wide observation field; all the investigated specimen length was observed in order to identify the crack initiation site. The investigated steps are $\epsilon_{\text{eng}} = 0\%$, 5%, 10%, and 14% (failure);
- 2) a diffractometer in order to evaluate XRD spectra. XRD measurements were made with a Philips X-PERT diffractometer equipped with a vertical Bragg–Brentano powder goniometer. A step–scan mode was used in the 2θ range from 40° to 90° with a step width of 0.02° and a counting time of 2 s per step. The employed radiation was monochromated $\text{CuK}\alpha$ (40 kV – 40 mA). The calculation of theoretical diffractograms and the generation of structure models were performed using the PowderCell software [8]. The investigated steps are at $\epsilon_{\text{eng}} = 0\%$ and 5%.



a) b)
Figure 1. Tensile equipment: a) loading frame, b) tensile machine.



a) b)
Figure 2. Etched surface: a) etched-deformed and observed, b) deformed, cleaned and re-etched.

Finally, SEM observations on fracture surface have been performed in order to evaluate the main fracture micromechanisms.

In order to check the correctness of the LOM observation procedure, a preliminary test has been performed. An unloaded and metallographically prepared specimen has been deformed up to $\epsilon_{\text{eng}}=0\%$ and then LOM observed (Fig. 2a). Subsequently the same specimen (loaded) has been metallographically prepared and LOM observed (Fig. 2b). It is evident the possibility to follow the grains modifications in the investigated SMA only performing the first metallographic preparation.

3. Results

Engineering stress strain curve of investigated alloy is shown in Fig. 3, where a plateau has not been observed. The investigated deformation conditions correspond to:

1. $\epsilon_{\text{eng}} = 0\%$ - starting test conditions;
2. $\epsilon_{\text{eng}} = 5\%$ - near yield point;
3. $\epsilon_{\text{eng}} = 10\%$ - plastic zone;
4. $\epsilon_{\text{eng}} = 14\%$ - specimen failure.

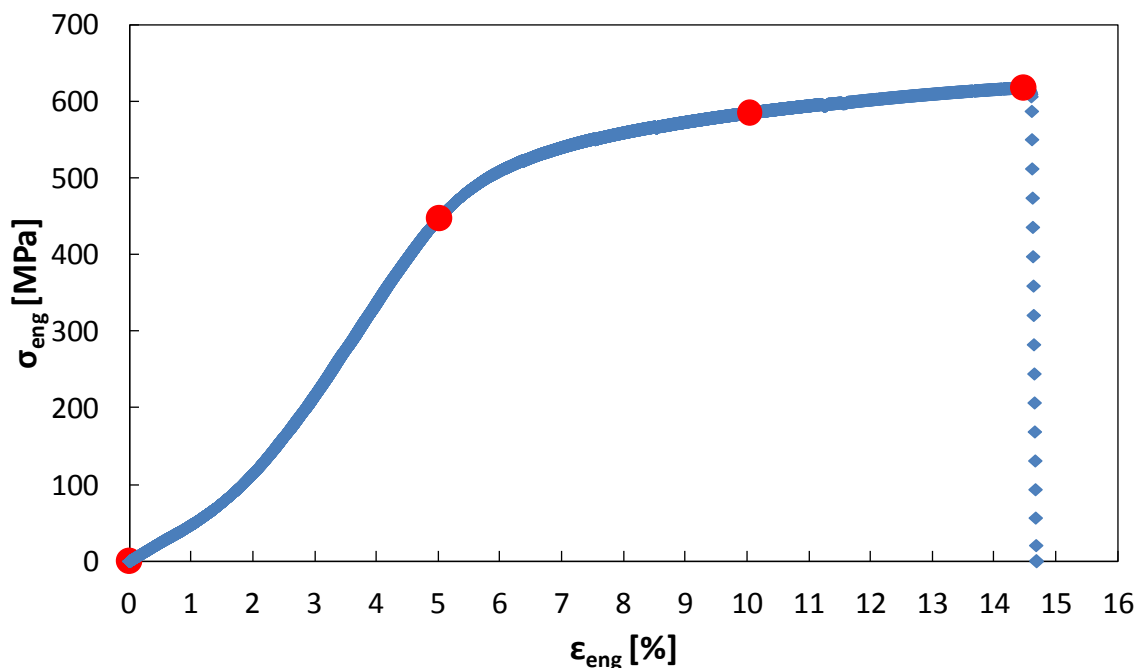


Figure 3. Engineering Stress-Strain curve (red points correspond to the investigated conditions).

The failure initiation site (Fig. 4), for $\epsilon_{\text{eng}} = 0\%$, is characterized by the presence of three grains (Fig. 4a). For $\epsilon_{\text{eng}} = 5\%$ (Fig. 4b) the three grains show an unchanged orientation, no sub-grains nucleation and a grain boundary deformation from linear to curved shape, probably due to phase transition. This is more evident in the grain on the left, where a surface modification is observed (sort of zig-zag lines on the surface). For $\epsilon_{\text{eng}} = 10\%$ (Fig. 4c), an intergranular crack initiate from the lateral specimen surface, with a secondary intergranular crack, that is more or less parallel to the applied load. This secondary crack is probably due to the phases transition in grains with different orientations, with a consequent τ stress increase at the grain boundary [7]. The increase of the macroscopical deformation implies an increase of the localized damage level, with the coalescence

of main and secondary cracks (Fig. 4d). Final failure is obtained by means of a crack propagation from one side to the opposite side of the specimen (“fracture ending zone”).

In Fig. 5, the “fracture ending zone” is shown. For $\epsilon_{eng} = 0, 5$ and 10% , corresponding respectively to Fig. 5a, b and c, no transformations are evident: surface modifications due to phase transformations are not observed in this zone. For $\epsilon_{eng} = 14\%$ (Fig. 5d), it is possible to observe a localized ductile deformation.

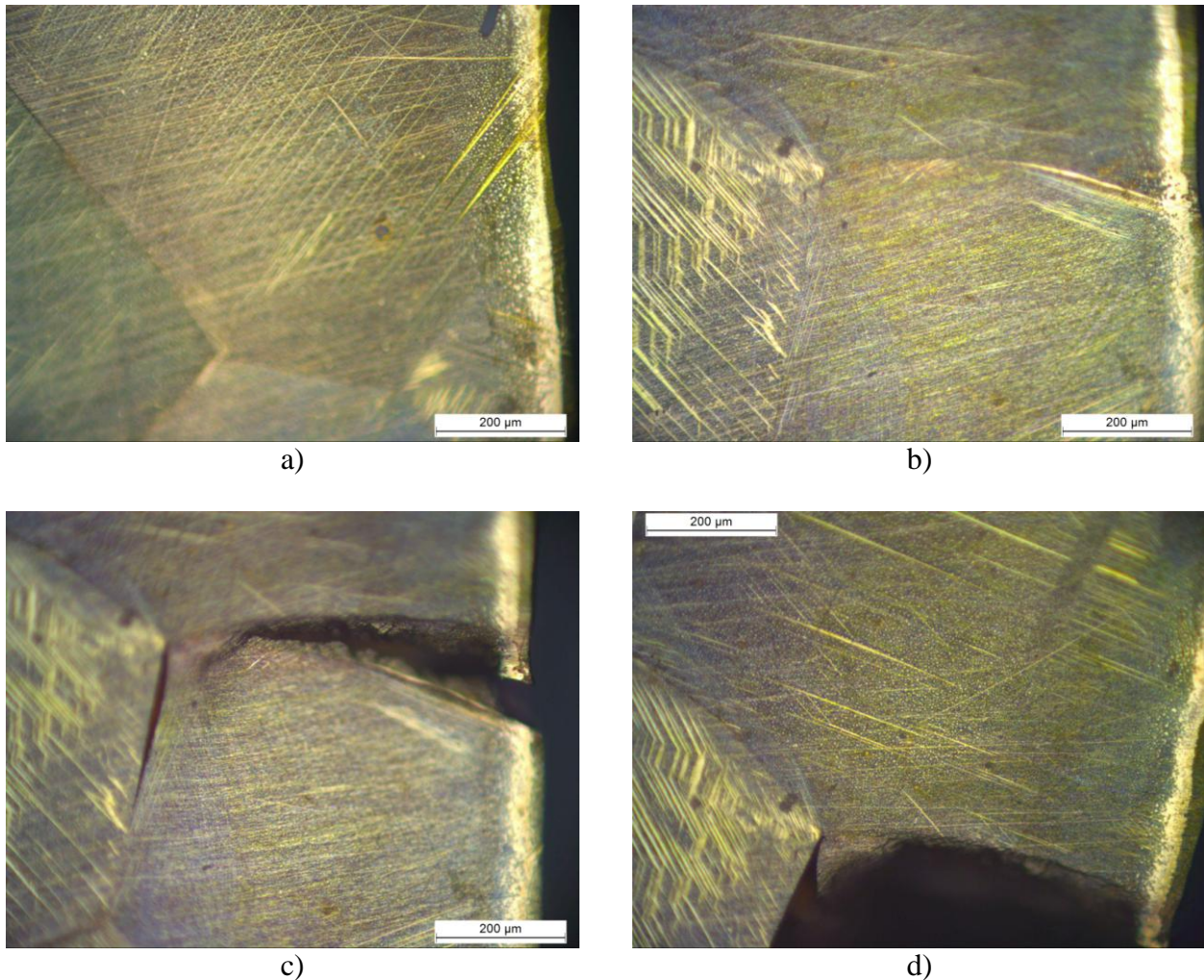


Figure 4. Fracture initiation zone: a) $\epsilon_{eng} = 0\%$, b) $\epsilon_{eng} = 5\%$, c) $\epsilon_{eng} = 10\%$, d) $\epsilon_{eng} = 14\%$ (failure).

Evidence of structure transitions are in Fig. 6, where two diffractograms show respectively the undeformed and the deformed at $\epsilon_{eng} = 5\%$ specimen. The undeformed specimen spectrum shows four peaks corresponding to $42.35^\circ, 43.71^\circ, 70.39^\circ, 80.23^\circ$. The $\epsilon_{eng} = 5\%$ deformed specimen shows also four peaks but corresponding to different diffraction angles ($42.27^\circ, 43.43^\circ, 43.85^\circ$ and 85.71°). Peaks modifications (considering both angles and intensity) show the mechanical deformation influence on the microstructure modifications.

Fracture surfaces are characterized by a brittle morphology, as the intergranular cleavage shown in Fig. 7a, which confirms the path observed on the lateral surface (Fig. 4c, d). According to the LOM damaging micromechanisms analysis and to SEM fracture surface analysis, grains decohesion seems to be main damaging micromechanisms.

Inclusions presence implies the initiation of secondary microcracks (Fig. 7b), probably due to the same mechanism which characterizes the grains decohesion.

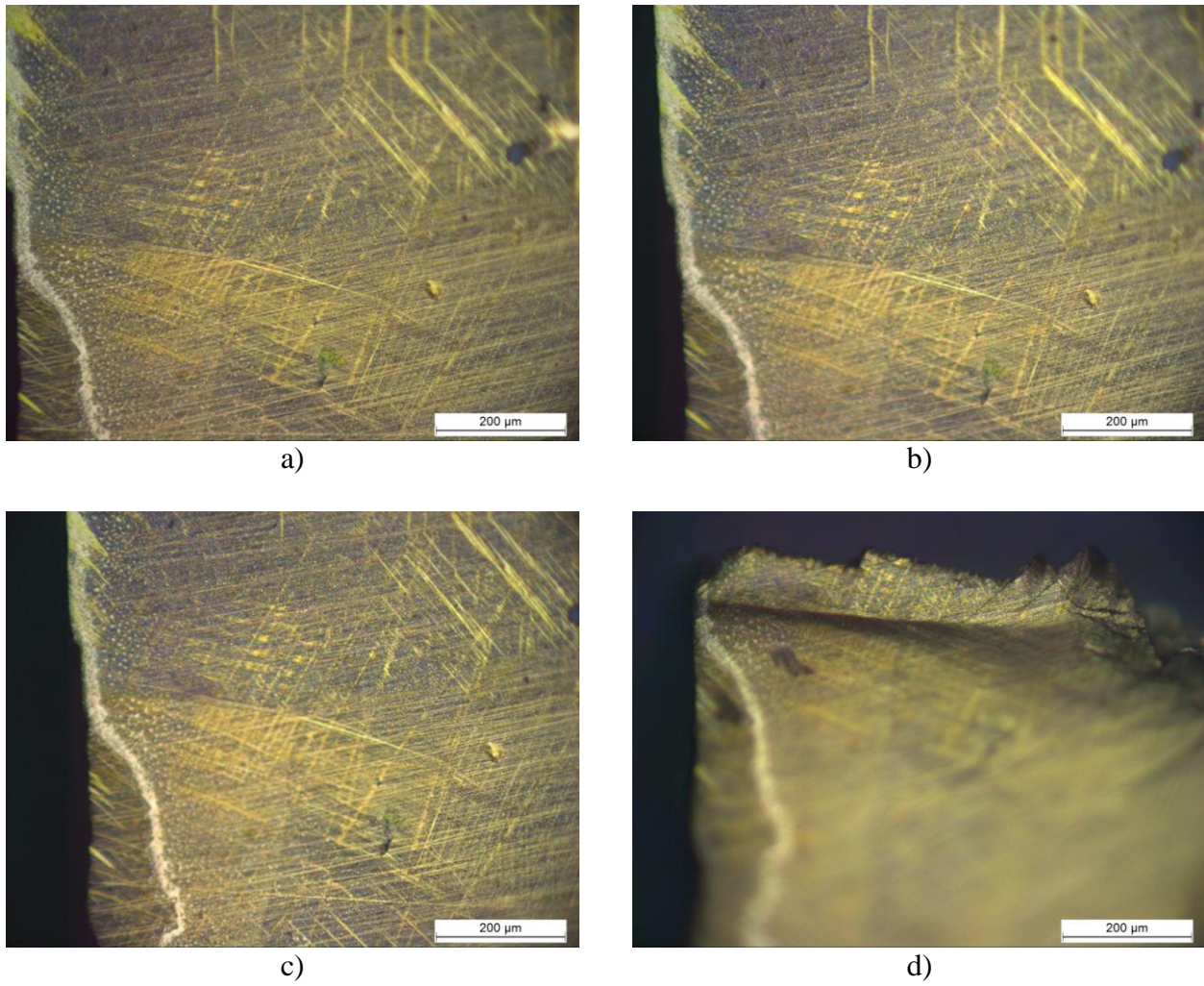


Figure 5. Fracture ending zone: a) $\epsilon_{eng} = 0\%$, b) $\epsilon_{eng} = 5\%$, c) $\epsilon_{eng} = 10\%$, d) $\epsilon_{eng} = 14\%$ (failure).

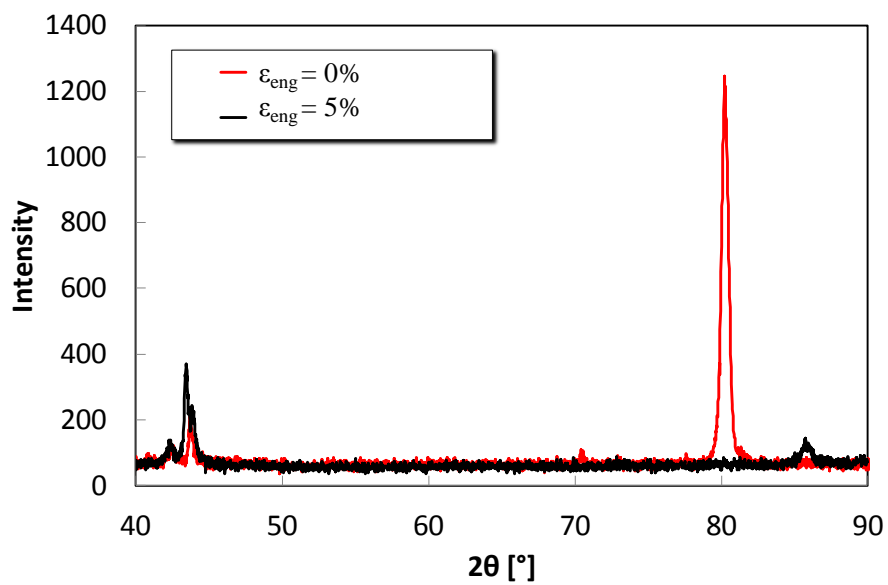


Figure 6. Diffraction spectra.

In the “ending fracture zone”, corresponding to the highest deformation values (Fig. 5d), ductile fracture micromechanisms are shown (Fig 8). Two ductile morphologies are observed in Fig. 8 (respectively indicated by arrows with letters A and B). Morphology in A is characterized by an oriented plastic deformation, while morphology in B is characterized by an unoriented deformation.

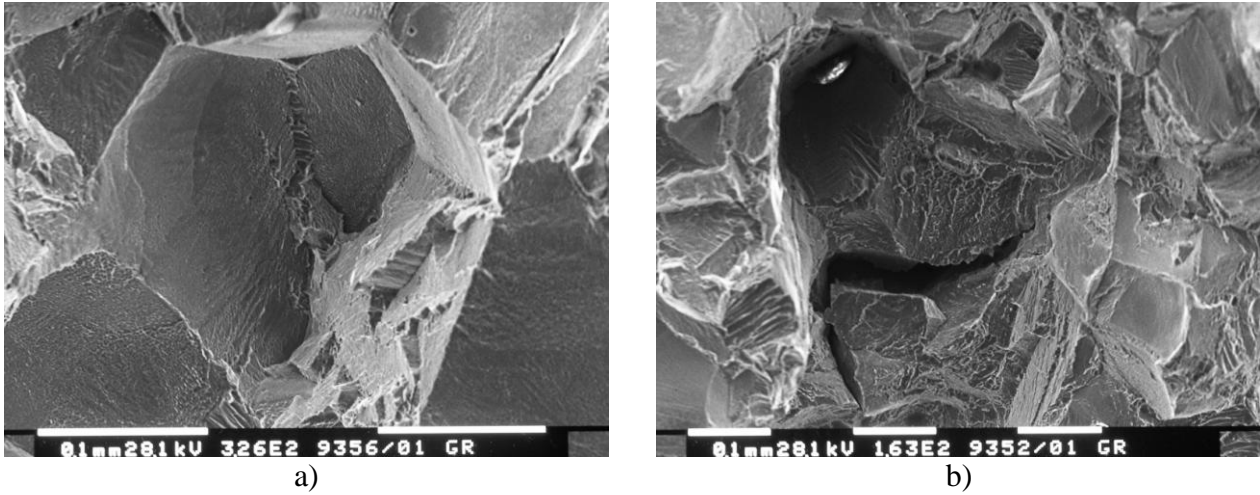


Figure 7. Fracture surface: a) intergranular cleavage, b) secondary crack in presence of inclusion.

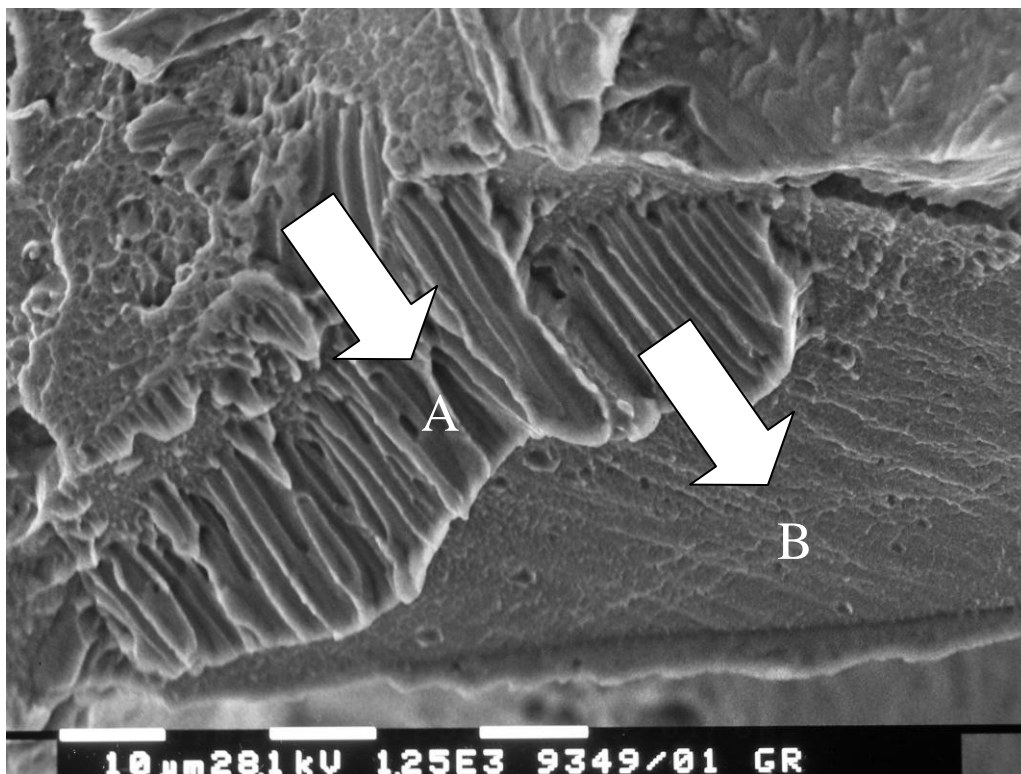


Figure 8. Fracture surface in the ending zone (as Fig. 5d)

Higher magnifications SEM observations (Fig. 9a and b) allow to confirm the ductile morphology of the fracture surface shown in Fig. 8.

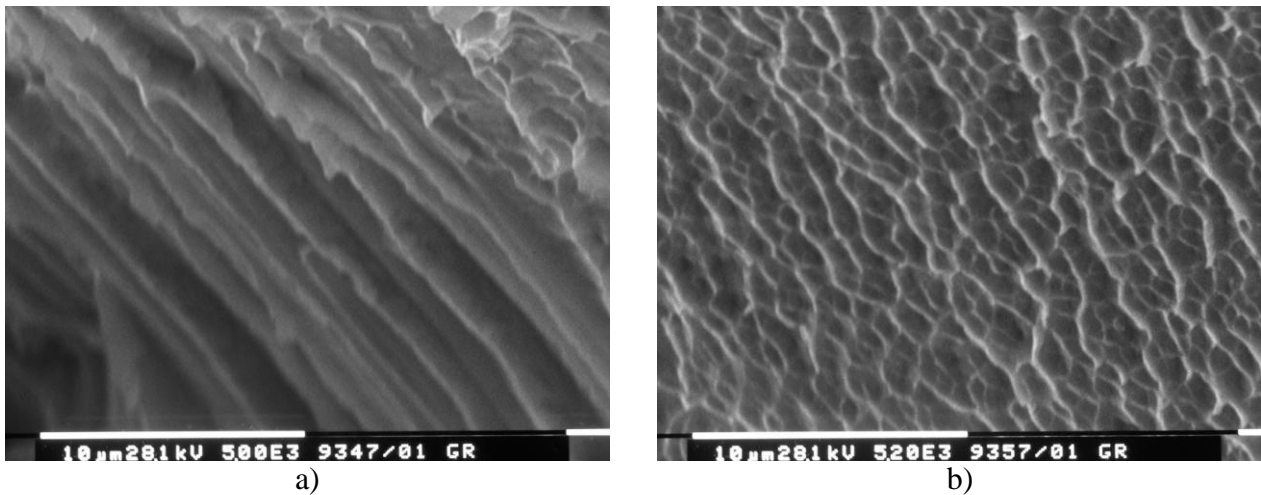


Figure 9. Fracture surface with high deformation: a) morphology of zone A of Fig. 8, b) morphology of zone B of Fig. 8.

4. Conclusions

In this work, the main crack initiation and propagation micromechanisms during tensile tests performed on a CuZnAl SMA has been analyzed. According to the experimental results, the following conclusions can be summarized:

- Cracks initiate at grains boundaries due both to high deformation values and to phases transitions;
- Memory effect is not only due to phases transitions, but also to the unchanging of numbers of grains boundary;
- The main fracture surface morphology is brittle and is characterized by intergranular cleavage;
- Corresponding to the highest deformation values (“ending fracture zone”) the main damaging micromechanism is ductile.

5. References

- [1] K. Otsuka, X. Ren, Physical metallurgy of Ti–Ni-based shape memory alloys, *Progress in Materials Science* (2005) 511.
- [2] Y. Dong, Z. Boming, L. Jun, A Changeable Aerofoil Actuated by Shape Memory Alloy Springs, *Materials Science and Engineering A*, 485 (2008) 243–250.
- [3] B. Chen, C. Liang, D. Fu, Pitting Corrosion of Cu–Zn–Al Shape Memory Alloy in Simulated Uterine Fluid, *J. Mater. Sci. Technology*, 21(2) (2005) 226-230.
- [4] Y. Liu, G.S. Tan, Formation of interfacial voids in cast and micro-grained γ' -Ni₃Al during high temperature oxidation, *Intermetallics* (2000) 8 1385-1391.
- [5] P. Arneodo Larochette, M. Ahlers, Grain-size dependence of the two-way shape memory effect obtained by stabilisation in Cu–Zn–Al crystals, *Materials Science and Engineering. A361* (2003) 249–257
- [6] N. Kayali, S. Ozgen, O. Adiguzel, Strain effects on the macroscopic behaviour and martensite morphology in shape-memory CuZnAl alloys, *Journal of Materials Processing Technology*. 101 (2000) 245-249.
- [7] J.X. Zhang, Y.F. Zheng, L.C. Zhao, The Structure and Mobility of Intervariant Boundaries in 18R Martensite in a Cu–Zn–Al Alloy, *Acta mater.* 47(7) (1999) 2125-2141.

- [8] PowderCell 2.3—Pulverdiffraktogramme aus Einkristalldaten und Anpassung experimenteller Beugungsaufnahmen, in http://www.bam.de/de/service/publikationen/powder_cell.htm.